Damage and noise sensitivity evaluation of autoregressive features extracted from structure vibration

2014 Smart Mater. Struct. 23 025007

(http://iopscience.iop.org/0964-1726/23/2/025007)

IOP Publishing Smart Materials and Structures
Smart Mater. Struct. **23** (2014) 025007 (15pp) doi:10.1088/0964-1726/23/2/025007

Damage and noise sensitivity evaluation of autoregressive features extracted from structure vibration

Ruigen Yao and Shamim N Pakzad

Department of Civil and Environmental Engineering, Lehigh University, Bethlehem, PA 18015, USA

E-mail: ruy209@Lehigh.edu

Received 25 June 2013, in final form 19 November 2013
Published 23 December 2013

Abstract
In the past few decades many types of structural damage indices based on structural health monitoring signals have been proposed, requiring performance evaluation and comparison studies on these indices in a quantitative manner. One tool to help accomplish this objective is analytical sensitivity analysis, which has been successfully used to evaluate the influences of system operational parameters on observable characteristics in many fields of study. In this paper, the sensitivity expressions of two damage features, namely the Mahalanobis distance of autoregressive coefficients and the Cosh distance of autoregressive spectra, will be derived with respect to both structural damage and measurement noise level. The effectiveness of the proposed methods is illustrated in a numerical case study on a 10-DOF system, where their results are compared with those from direct simulation and theoretical calculation.

Keywords: sensitivity analysis, structural vibration monitoring, autoregressive modeling, autoregressive spectrum estimation, Yule–Walker method

(Some figures may appear in colour only in the online journal)

1. Introduction

Damage detection is a very crucial part in the regular assessment and maintenance routine for civil infrastructure. Traditionally this task is carried out by human inspection, and thereby is expensive, time-consuming and the accuracy relies on individual expertise. Recently, the advancements in sensing and computational technology have made it feasible for a sensor network to be installed on a civil structure, and data collected from the sensors will then be processed to produce information pertaining to the structural condition. To date many research studies in the literature [1–4] devoted to this topic can be found, forming a promising branch of study often referred to as data-driven structural health monitoring (SHM). Ideally, the new system will cost less than traditional methods because of the lowering prices of sensing systems, and produce more accurate and reliable decisions that are free of human judgment bias or expertise. Moreover, SHM has the capability to reveal problems undetectable via 'naked-eye' inspection such as internal fracture and delamination.

Vibration responses (e.g. acceleration, strain) are among the most commonly measured signals for structural monitoring purposes. One category of widely employed vibration-based damage indices consists of modal properties extracted using system identification/modal realization approaches [5–7]. Recently, many alternative damage features [8–10] based on structural output are proposed to address the computational efficiency issues (especially for time domain extraction algorithms) concerning modal properties estimators [1]. Time series analysis [11] for single channel acceleration measurements is one of the notable techniques attempted in a number of research articles [12–17], where algorithms such as scalar autoregressive (AR), autoregressive/autoregressive with exogenous input (AR–ARX) and autoregressive with moving average (ARMA) modeling have been applied and functions of estimated model parameters used as damage features. These features are reported to be less complicated to compute and more sensitive to local damage in their respective applications. References [13, 16] provide comparisons on the effect of local damage on the

modal frequencies/shapes and autoregressive features, and it is observed in both case studies that the latter shows a more noticeable change than the former. Also, the AR–ARX method has demonstrated success in damage localization in [13] and the ARMA method has been used to indicate damage location and extent in [15]. The AR methods, however, are not sensitive to damage location [17]. It is noted that univariate time series analysis methods are output only, and damage indices of this type are often functions of structural signal autocovariance functions, which are in turn determined by the structural stiffness properties, the structural geometry and excitation patterns. When the location of damage does not correspond well with where the largest damage-induced change in signal autocovariance functions occurs, damage localization based on time series analysis is likely to be very difficult. Still, these damage features have advantages such as being simple in concept, convenient for statistical processing as they can be generated in large quantities, and suitable for decentralized structural monitoring applications.

While it is important to propose and test new features to improve the state-of-the-art of structural damage detection, examination of the effect of structural change and environmental and operational factors on existing features in an analytically rigorous manner is also crucial for optimal feature selection for different practices. Previously, research has been conducted on evaluating the adverse effect of measurement noise on the accuracy of estimated modal parameters [18]. In this paper, the sensitivity of two damage features based on AR modeling due to damage level and measurement noise is studied and an analysis methodology is proposed. The two methods are the Mahalanobis distance [19] of AR coefficients and the Cosh distance [20] of AR model spectra between the baseline state and the current state. The validity of this methodology is supported by simulation results from a 10-DOF bridge model.

The paper is organized as follows. Section 2 gives an explanation of the theoretical relation between the structural acceleration response and the family of AR modeling, together with an examination of the properties of the scalar Yule–Walker AR coefficient estimators. Section 3 contains stepwise derivations regarding the analysis for the sensitivity with respect to damage level and measurement noise for both features. In section 4, sensitivity analysis is applied to a 10-DOF simulated model and the results are compared with those from direct simulation and theoretical calculation. Conclusions are then made on the efficiency of the algorithms and the effectiveness of the features.

2. Autoregressive modeling for structural vibration measurements

As noted in the introduction, sensor measurements do not reveal information concerning the structural state being monitored until they go through data-processing algorithms. Autoregressive (AR) modeling is one of the most effective time series analysis techniques and has found applications in vibration monitoring of various types of structures [8, 13, 15] that are instrumented with accelerometers. Here, different aspects of AR modeling are investigated in two sections. Section 2.1 demonstrates the validity of AR modeling for structural vibration signals and presents a proof on a multi-input–multi-output (MIMO) ARX model between the excitation and acceleration response of a MDOF system. Since univariate AR estimators tend to behave differently from their multivariate counterparts because of the spatial correlation among structural responses, section 2.2 investigates the characteristics of single-input–single-output (SISO) AR coefficient estimators from acceleration measurements to provide insight into the behavior of the autoregressive features thus extracted.

2.1. Civil structural systems and AR/ARX model

An ARX model is a numerical tool that has been proved quite useful in describing causal systems subjected to a series of external disturbances [21]. In an effort to derive an explicit ARX model for a N-degrees-of-freedom system between its excitation source and acceleration measurements, the system impulse response should be obtained, discretized and transformed. To start, calculate the acceleration impulse response of the ith mode by twice differentiating Duhamel's integral of the displacement impulse response $h_i(t)$ [22]:

$$\begin{aligned}\ddot{h}_i(t) &= \frac{\mathrm{d}^2\{\int_0^t h_i(t-\tau)\delta(\tau)\,\mathrm{d}\tau\}}{\mathrm{d}t^2}\\ &= h_i(0)\delta'(t) + h_i'(t-\tau)\delta(\tau)|_{\tau=t}\\ &\quad + \int_0^t \frac{\mathrm{d}^2}{\mathrm{d}t^2}\{h_i(t-\tau)\}\delta(\tau)\,\mathrm{d}\tau, \end{aligned} \tag{1}$$

where $\delta(\tau)$ here stands for the Dirac delta function. The acceleration impulse response may be written as the sum of the second-order derivative of the displacement impulse response and an impulse term:

$$\begin{aligned}\ddot{h}_i(t) &= \frac{\mathrm{d}^2[h_i(t)]}{\mathrm{d}t^2} + \frac{1}{m_i}\delta(t)\\ &= \frac{-\omega_{\mathrm{D}i}^2}{m_i\omega_{\mathrm{D}i}}\mathrm{e}^{-\zeta_i\omega_{\mathrm{n}i}t}\sin\omega_{\mathrm{D}i}t\\ &\quad + \frac{-2\zeta_i\omega_{\mathrm{D}i}\omega_{\mathrm{n}i}}{m_i\omega_{\mathrm{D}i}}\mathrm{e}^{-\zeta_i\omega_{\mathrm{n}i}t}\cos\omega_{\mathrm{D}i}t\\ &\quad + \frac{\zeta_i^2\omega_{\mathrm{n}i}^2}{m_i\omega_{\mathrm{D}i}}\mathrm{e}^{-\zeta_i\omega_{\mathrm{n}i}t}\sin\omega_{\mathrm{D}i}t + \frac{1}{m_i}\delta(t) \end{aligned} \tag{2}$$

where m_i, $\omega_{\mathrm{n}i}, \omega_{\mathrm{D}i}$ and ζ_i are the modal mass, natural frequency, damped frequency and damping ratio of the ith mode, respectively. The discretized version of equation (2) is

$$\begin{aligned}a_i[n] &= \frac{-\omega_{\mathrm{D}i}^2}{m_i\omega_{\mathrm{D}i}}\mathrm{e}^{-\zeta_i\omega_{\mathrm{n}i}T_{\mathrm{s}}n}\sin\omega_{\mathrm{D}i}T_{\mathrm{s}}n\\ &\quad + \frac{-2\zeta_i\omega_{\mathrm{D}i}\omega_{\mathrm{n}i}}{m_i\omega_{\mathrm{D}i}}\mathrm{e}^{-\zeta_i\omega_{\mathrm{n}i}T_{\mathrm{s}}n}\cos\omega_{\mathrm{D}i}T_{\mathrm{s}}n\\ &\quad + \frac{\zeta_i^2\omega_{\mathrm{n}i}^2}{m_i\omega_{\mathrm{D}i}}\mathrm{e}^{-\zeta_i\omega_{\mathrm{n}i}T_{\mathrm{s}}n}\sin\omega_{\mathrm{D}i}T_{\mathrm{s}}n + \frac{1}{m_iT_{\mathrm{s}}}\delta(n) \end{aligned} \tag{3}$$

where n is the time label in the discrete domain and T_s is the sampling interval. Its corresponding z-transform can be obtained as

$$\begin{aligned}\hat{a}(z) = &\left(\frac{-\omega_{Di}^2}{m_i\omega_{Di}} + \frac{\zeta_i^2\omega_{ni}^2}{m_i\omega_{Di}}\right)\\ &\times \frac{e^{-\zeta_i\omega_{ni}T_s}z^{-1}\sin\omega_{Di}T_s}{1-2e^{-\zeta_i\omega_{ni}T_s}z^{-1}\cos\omega_{Di}T_s + e^{-2\zeta_i\omega_{ni}T_s}z^{-2}}\\ &+ \frac{-2\zeta_i\omega_{Di}\omega_{ni}}{m_i\omega_{Di}}\\ &\times \frac{1-e^{-\zeta_i\omega_{ni}T_s}z^{-1}\cos\omega_{Di}T_s}{1-2e^{-\zeta_i\omega_{ni}T_s}z^{-1}\cos\omega_{Di}T_s + e^{-2\zeta_i\omega_{ni}T_s}z^{-2}}\\ &+ \frac{1}{m_iT_s}. \end{aligned} \tag{4}$$

Defining the discretized modal input/output as $q_i[n]$ and $p_i[n]$, their relation can be expressed using an ARX model by taking the inverse z-transform and rearranging equation (4):

$$\begin{aligned}&q_i[n] - 2e^{-\zeta_i\omega_{ni}T_s}\cos\omega_{D_i}T_s q_i[n-1] + e^{-2\zeta_i\omega_{ni}T_s}q_i[n-2]\\ &= \left(\frac{1}{m_iT_s} - \frac{2\zeta_i\omega_{ni}}{m_i}\right)p_i[n] + e^{-\zeta_i\omega_{ni}T_s}\left[\frac{-2\cos\omega_{D_i}T_s}{m_iT_s}\right.\\ &+ \sin\omega_{Di}T_s\left(\frac{-\omega_{Di}}{m_i} + \frac{\zeta_i^2\omega_{ni}^2}{m_i\omega_{Di}}\right)\\ &\left.+ \cos\omega_D T_s\frac{2\zeta_i\omega_{ni}}{m_i}\right]p_i[n-1]\\ &+ \frac{e^{-2\zeta_i\omega_{ni}T_s}}{m_iT_s}p_i[n-2]. \end{aligned} \tag{5}$$

For notational simplicity the coefficient expressions will be omitted for now and equation (5) is denoted as

$$\begin{aligned}&A_i(B)q_i[n] = C_i(B)p_i[n],\\ &B\text{: the backshift operator, i.e. } Bp[n] = p[n-1]. \end{aligned} \tag{6}$$

For the MDOF model discussed here, the matrix form of representation can be employed:

$$\mathbf{A}(B)\mathbf{q}[n] = \mathbf{C}(B)\mathbf{p}[n], \tag{7}$$

where $\mathbf{A}(B)$ and $\mathbf{C}(B)$ are diagonal matrices consisting of $A_i(B)$ and $C_i(B)$ terms, respectively. $\mathbf{q}[n]$ is the modal displacement vector and $\mathbf{p}[n]$ is the modal input vector. Their relationship with the nodal input vector $\mathbf{x}[n]$ and nodal displacement vector $\mathbf{y}[n]$ are as follows:

$$\mathbf{y}[n] = \mathbf{\Phi}\mathbf{q}[n], \qquad \mathbf{x}[n] = \mathbf{\Phi}^{T^{-1}}\mathbf{p}[n] \tag{8}$$

where $\mathbf{\Phi}$ here stands for the system eigenvector matrix. Therefore, the relation between the excitation and system acceleration response can be expressed as a multivariate ARX model:

$$\begin{aligned}&\mathbf{A}'(B)\mathbf{y}[n] = \mathbf{C}'(B)\mathbf{x}[n],\\ &\mathbf{A}'(B) = \mathbf{\Phi}\mathbf{A}(B)\mathbf{\Phi}^{-1}, \qquad \mathbf{C}'(B) = \mathbf{\Phi}\mathbf{C}(B)\mathbf{\Phi}^{T}. \end{aligned} \tag{9}$$

Note that $\mathbf{A}'(0) = \mathbf{\Phi}\mathbf{A}(0)\mathbf{\Phi}^{-1} = \mathbf{\Phi}\mathbf{\Phi}^{-1} = \mathbf{I}$. For signals generated from the multivariate ARX system under random excitation, each scalar signal can be viewed as a sum of seemingly uncorrelated ARMA processes and modeled with a scalar ARMA process [23].

2.2. AR coefficient estimators for scalar acceleration signals

ARMA processes can be approximated with an AR process with a large model order [24]. One main advantage of the latter method is its computational efficiency. The definition of a univariate AR model of order p is

$$x(t) = \sum_{j=1}^{p}\varphi_j x(t-j) + \eth_x(t). \tag{10}$$

In this equation, $x(t)$ is the time series to be analyzed, φ_j terms are the AR model coefficients and $\eth_x(t)$ is the model residual. Because of its concise form, the AR model has been widely adopted for time series analysis for different purposes. One of the frequently used AR coefficient estimators is the Yule–Walker estimator [24], which is obtained from solving the following equation:

$$\begin{aligned}\begin{bmatrix}\hat{\varphi}_1\\ \hat{\varphi}_2\\ \hat{\varphi}_3\\ \vdots\\ \hat{\varphi}_p\end{bmatrix} &= \begin{bmatrix}R(0) & R(1) & R(2) & \cdots & R(p-1)\\ R(1) & R(0) & R(1) & \cdots & R(p-2)\\ R(2) & R(1) & R(0) & \cdots & R(p-3)\\ \vdots & \vdots & \vdots & \ddots & \vdots\\ R(p-1) & R(p-2) & R(p-3) & \cdots & R(0)\end{bmatrix}^{-1}\\ &\times \begin{bmatrix}R(1)\\ R(2)\\ R(3)\\ \vdots\\ R(p)\end{bmatrix} = \Gamma^{-1}\gamma, \end{aligned} \tag{11}$$

where $R(\cdot)$ is the autocovariance function (ACF) of the time series and $\{\hat{\varphi}_j\}$ are the AR coefficients.

When an AR model (which is an all-pole system) is constructed from the structural acceleration signal, spurious poles will be introduced because the model cannot properly parameterize possible zeros in the underlying generating function, leading to a large AR order for an accurate model:

$$\begin{aligned}1-\beta z^{-1} &\approx \frac{1-\beta z^{-1}}{1-\beta^{n+1}z^{-(n+1)}}\\ &= \frac{1}{1+\beta z^{-1}+\cdots+\beta^n z^{-n}},\\ &\quad (|\beta z^{-1}|<1)\\ 1-\beta z^{-1} &\approx \frac{-\beta z^{-1}(1-\beta^{-1}z)}{1-\beta^{-(n+1)}z^{n+1}}\\ &= \frac{-\beta^{n+1}z^{-(n+1)}}{1+\beta z^{-1}+\cdots+\beta^n z^{-n}},\\ &\quad (|\beta z^{-1}|>1). \end{aligned} \tag{12}$$

In either case the pole positions should be inside the unit circle to ensure a stable system. Poles thus generated tend to be uniformly distributed around the unit circle. Figure 1 shows the ACF and the pole location plots in the z plane of

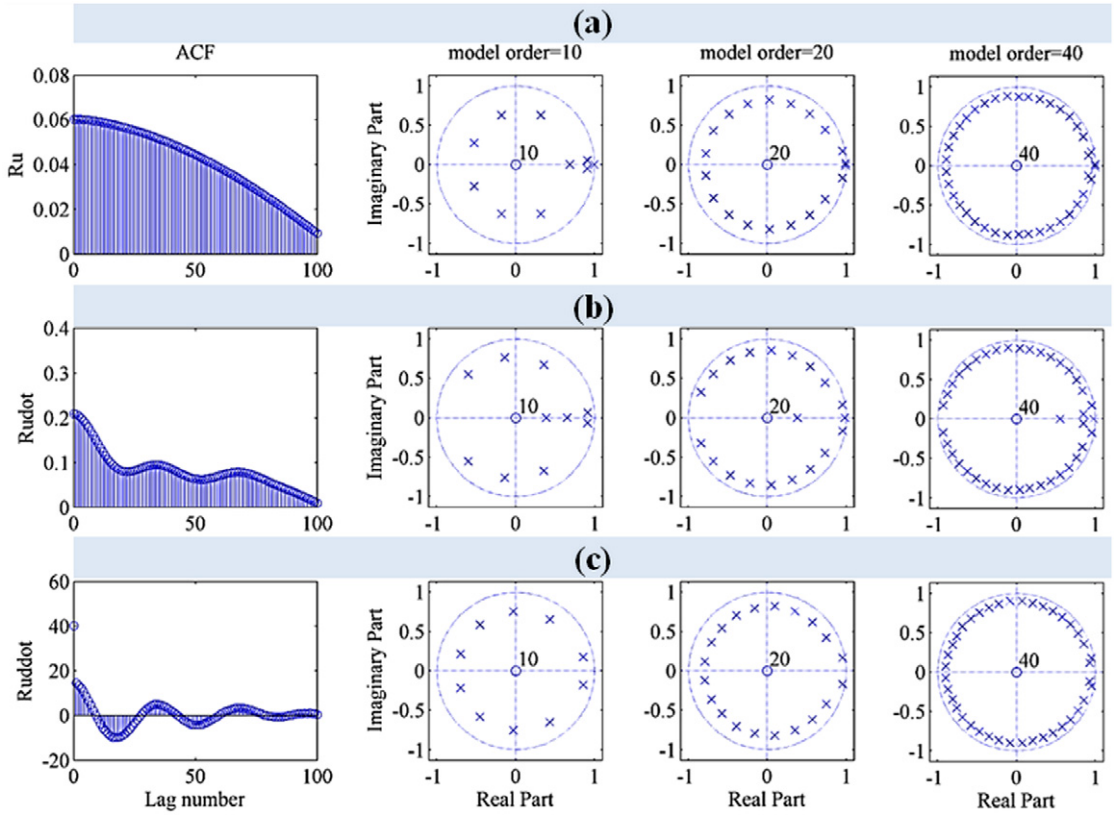

Figure 1. Pole positions of AR model estimated from structural displacement (a), velocity (b) and acceleration (c) signals. The first column of the subplots shows the ACF values, while the rest displays the pole positions of different models in the z plane.

Yule–Walker estimators for structural displacement, velocity and acceleration signals. Compared with the poles of models based on the displacement and velocity, the poles of models based on the acceleration have a more balanced distribution inside the unit circle even at low AR orders. This is because the ACF of acceleration measurements has a large impulse term at zero lag, which has a uniform frequency domain response and is a characteristic of white noise. Since the AR model is a 'whitening' filter by definition [21], the poles from a model estimated using such a signal should have relatively evenly distributed poles around the origin to achieve a relatively 'flat' model spectrum. Also note that, as the model order increases, the pole positions move closer to the unit circle as the estimated system becomes less stable.

A brief explanation on this phenomenon is presented here: in the case of Yule–Walker estimation, the AR estimator of order $p+1$ is related to an estimator of order p as

$$\begin{aligned}&[\hat{\varphi}_{1,p+1}, \hat{\varphi}_{2,p+1}, \ldots, \hat{\varphi}_{p+1,p+1}]\\ &\quad = [\hat{\varphi}_{1,p}, \hat{\varphi}_{2,p}, \ldots, \hat{\varphi}_{p,p}, 0]\\ &\quad - K_{p+1}[\hat{\varphi}_{p,p}, \hat{\varphi}_{p-1,p}, \ldots, \hat{\varphi}_{1,p}, -1]\end{aligned} \tag{13}$$

where $\hat{\varphi}_{i,p}$ denotes the ith estimated coefficient for an AR model of order p and K_{p+1} is the $(p+1)$th-order partial correlation coefficient [24] of the estimated signal. If the signal is strictly autoregressive up to lag p, then the expected value of K_{p+1} is zero. However, because the ambient structural vibration signals are ARMA processes, this condition generally can only be satisfied in the asymptotic sense. As such, the AR coefficient vector will vary as a whole as the model order increases and so does the corresponding model spectra estimates:

$$\begin{aligned}\hat{S}^{p}_{\mathrm{AR}}(\omega) &= \frac{d_p}{|1-\sum_{k=1}^{p}\hat{\varphi}_{k,p}\mathrm{e}^{-\mathrm{j}\omega k}|^2}\\ &= \frac{d_p}{|(1-\alpha_{1,p}\mathrm{e}^{-\mathrm{j}\omega})\ldots(1-\alpha_{p,p}\mathrm{e}^{-\mathrm{j}\omega})|^2},\\ \hat{S}^{p+1}_{\mathrm{AR}}(\omega) &= \frac{d_{p+1}}{|1-\sum_{k=1}^{p+1}\hat{\varphi}_{k,p+1}\mathrm{e}^{-\mathrm{j}\omega k}|^2}\\ &= \frac{d_p(1-K_{p+1}^2)}{|(1-\alpha_{1,p+1}\mathrm{e}^{-\mathrm{j}\omega})\ldots(1-\alpha_{p+1,p+1}\mathrm{e}^{-\mathrm{j}\omega})|^2}\\ &= [d_p(1-K_{n+1}^2)][|(1-\alpha_{1,p}\mathrm{e}^{-\mathrm{j}\omega})\\ &\quad \ldots(1-\alpha_{p,p}\mathrm{e}^{-\mathrm{j}\omega}) - K_{p+1}\mathrm{e}^{-\mathrm{j}\omega}(\mathrm{e}^{-\mathrm{j}\omega}-\alpha_{1,p})\\ &\quad \ldots(\mathrm{e}^{-\mathrm{j}\omega}-\alpha_{p,p})|^2]^{-1}.\end{aligned} \tag{14}$$

Here $\alpha_{i,p}$ stands for the ith pole of the AR model of order p. Note that the nominal input power d_p decreases as model order increases, which led to the shift of pole positions to the unit circle so that the output amplitude can still remain at the same level given a weaker input. It can be proved that the complex numbers $(1-\alpha_1\mathrm{e}^{-\mathrm{j}\omega})\ldots(1-\alpha_p\mathrm{e}^{-\mathrm{j}\omega})$ and $(\mathrm{e}^{-\mathrm{j}\omega}-\alpha_1)\ldots(\mathrm{e}^{-\mathrm{j}\omega}-\alpha_p)$ have the same magnitude, but different phases [25]. The expression for $\hat{S}^{p+1}_{\mathrm{AR}}(\omega)$ is thus

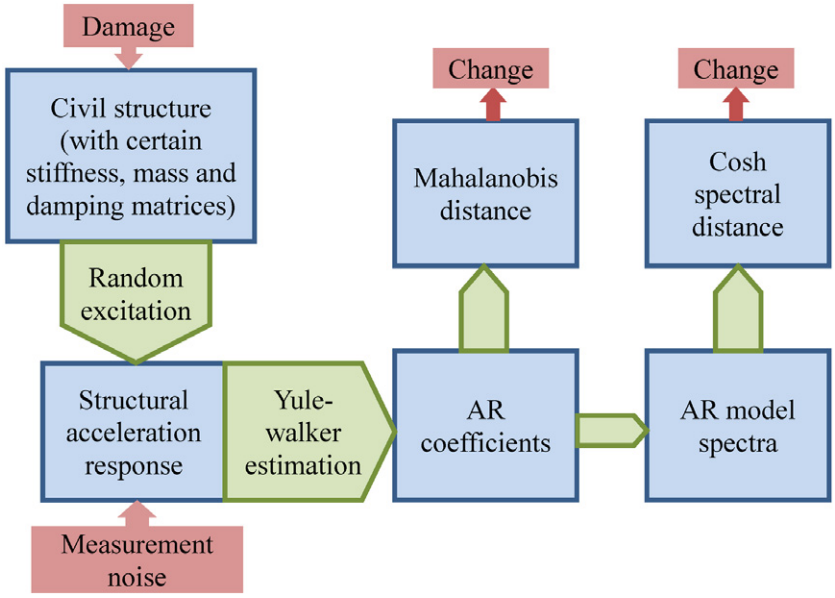

Figure 2. Illustration of the relation between structural damage/measurement noise and AR-based damage features.

further simplified as

$$\begin{aligned}
&\hat{S}_{\mathrm{AR}}^{p+1}(\omega) \\
&= \frac{d_p(1-K_{p+1}^2)}{|1-K_{p+1}\mathrm{e}^{-\mathrm{j}\Omega(\omega)}|^2|(1-\alpha_1\mathrm{e}^{-\mathrm{j}\omega})\ldots(1-\alpha_p\mathrm{e}^{-\mathrm{j}\omega})|^2} \\
&= \frac{(1-K_{p+1}^2)\hat{S}_{\mathrm{AR}}^{p}(\omega)}{|1-K_{p+1}\mathrm{e}^{-\mathrm{j}\Omega(\omega)}|^2}, \\
&\Omega(\omega) \\
&= \angle\frac{(1-\alpha_{1,p}\mathrm{e}^{-\mathrm{j}\omega})\ldots(1-\alpha_{p,p}\mathrm{e}^{-\mathrm{j}\omega})}{\mathrm{e}^{-\mathrm{j}\omega}(\mathrm{e}^{-\mathrm{j}\omega}-\alpha_{1,p})\ldots(\mathrm{e}^{-\mathrm{j}\omega}-\alpha_{p,p})} \\
&= (p+1)\omega + 2\angle(1-\alpha_{1,p}\mathrm{e}^{-\mathrm{j}\omega})\ldots(1-\alpha_{p,p}\mathrm{e}^{-\mathrm{j}\omega}).
\end{aligned} \tag{15}$$

When K_{p+1} is significantly small, the pole positions of the AR spectrum will not change much as the model order increases and the spectrum shape will converge.

3. Damage level and measurement noise sensitivity for the AR damage features

Distance measures between characteristics of undamaged and damaged structure states are often adopted as damage features. Damage features examined in this paper are the Mahalanobis distance of AR coefficients and the Cosh distance of AR model spectra extracted from structural acceleration measurements [14]. The Mahalanobis distance is a metric to evaluate the deviation within vectorial Gaussian sample groups [19]. Its definition is stated as below:

$$D^2(\boldsymbol{\varphi}_{\mathrm{u}}, \bar{\boldsymbol{\varphi}}_{\mathrm{b}}) = (\boldsymbol{\varphi}_{\mathrm{u}}^{\mathrm{T}} - \bar{\boldsymbol{\varphi}}_{\mathrm{b}}^{\mathrm{T}})\boldsymbol{\Sigma}_{\mathrm{b}}^{-1}(\boldsymbol{\varphi}_{\mathrm{u}} - \bar{\boldsymbol{\varphi}}_{\mathrm{b}}) \tag{16}$$

where $\boldsymbol{\varphi}_{\mathrm{u}}$ is the feature vector (in this case, the AR coefficients) from the unknown structural state and $\bar{\boldsymbol{\varphi}}_{\mathrm{b}}/\boldsymbol{\Sigma}_{\mathrm{b}}$ is the mean/covariance of feature vectors from the baseline state. When the unknown vector $\boldsymbol{\varphi}_{\mathrm{u}}$ is not generated from the baseline distribution, it is expected that the distance value will increase significantly.

From each vector of AR coefficients, a corresponding AR spectrum plot can be constructed:

$$S_{\mathrm{AR}}^{(p)}(\omega) = \frac{\sigma_{\mathrm{e}}^2}{|\boldsymbol{\varphi}(\mathrm{e}^{\mathrm{j}\omega})|^2} = \frac{\sigma_{\mathrm{e}}^2}{\left|\sum_{k=0}^{p}\varphi_k\mathrm{e}^{-\mathrm{j}\omega k}\right|^2}, \tag{17}$$

where $\varphi_0 = 1$. For feature extraction purposes the model residual variance σ_{e}^2 is not calculated and set to unity, since its value is determined by excitation level. The Cosh spectral distance based on AR spectrum estimates can be used as a frequency domain alternative to the Mahalanobis distance of AR coefficients:

$$C(\mathbf{S}, \bar{\mathbf{S}}_{\mathrm{b}}) = \frac{1}{2N}\sum_{j=1}^{N}\left[\frac{S(\omega_j)}{\bar{S}_{\mathrm{b}}(\omega_j)} + \frac{\bar{S}_{\mathrm{b}}(\omega_j)}{S(\omega_j)} - 2\right] \tag{18}$$

where $\bar{\mathbf{S}}_{\mathrm{b}}$ is the baseline spectrum, $\mathbf{S}$ is the spectrum from the unknown state and N is the length of each spectrum vector. An illustration of the procedures through which the features are generated is also given in figure 2. The features are related to the structural damage through the autocorrelation function of acceleration signals, which is determined by structural stiffness properties and excitation characteristics. The analytical relation between the features and structural damage/measurement noise is explored in the remainder of this section, where noise/damage sensitivity of both indices are derived in four steps because the relation is not an evident one.

3.1. Sensitivity of structural response ACF to damage

An AR model is an all-pole system. From equation (5) it is observed that the ith mode of the N-degrees-of-freedom system corresponds to a conjugate pair of system poles:

$$z_i, z_i^* = \mathrm{e}^{-\zeta_i\omega_{\mathrm{n}i}T_{\mathrm{s}} \pm \mathrm{j}\sqrt{1-\zeta_i^2}\omega_{\mathrm{n}i}T_{\mathrm{s}}}. \tag{19}$$

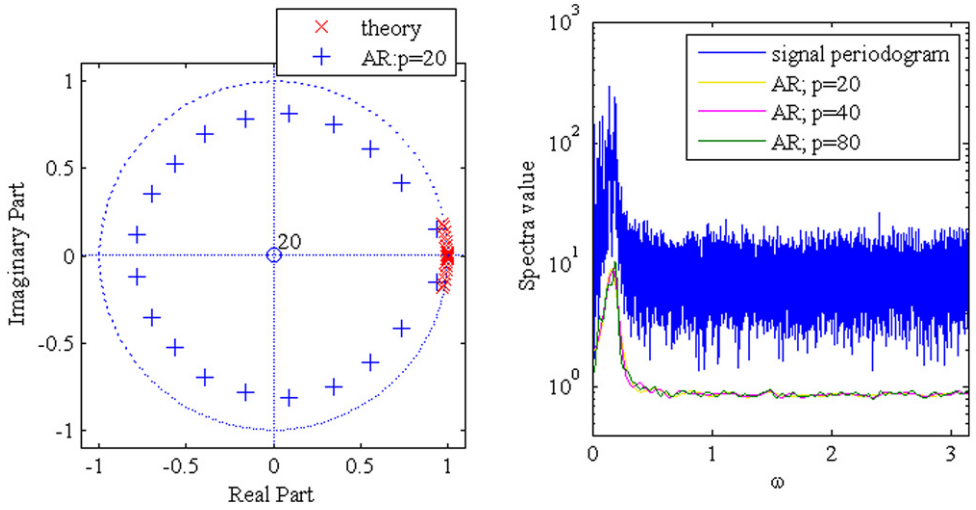

Figure 3. The contrast of the theoretical pole positions from digital signal processing theory and those from estimated AR models (left plot) and the comparison of the signal periodogram and the AR model spectra of different orders (right plot).

If it is assumed that the estimated AR model exactly captures all system poles, then an AR coefficient vector of size $(2N \times 1)$ can be computed by utilizing relations between polynomial coefficients and roots. However, simulation analysis reveals that there is a very large difference between the theoretical poles and those estimated from AR modeling (figure 3). Also noted from figure 3 is that the AR spectrum does not converge to resemble the envelope of signal periodogram as the model order increases. Therefore, the damage sensitivity of the system ACF, from which the AR coefficient estimators are computed through equation (11), is investigated here as a first step towards obtaining accurate sensitivity estimates for both features.

To start, take the Laplace transform of the displacement impulse response of the ith system mode:

$$h_i(t) = \frac{1}{m_i \omega_{\mathrm{D}i}} \mathrm{e}^{-\zeta_i \omega_{\mathrm{n}i} t} \sin \omega_{\mathrm{D}i} t.$$
$$\overset{\text{L.T.}}{\Rightarrow} \hat{h}_i(s) = \frac{1}{m_i (s^2 + 2\zeta_i \omega_{\mathrm{n}i} s + \omega_{\mathrm{n}i}^2)}. \tag{20}$$

From the relationship between modal and nodal input/response in structural dynamics the impulse response matrix and the Laplace transfer function of the whole system can be obtained as

$$\begin{aligned} \mathbf{H}(t) &= \mathbf{\Phi} \mathrm{diag}\,(h_i(t)) \mathbf{\Phi}^{\mathrm{T}}, \\ \hat{\mathbf{H}}(s) &= \mathbf{\Phi} \mathrm{diag}\,(\hat{h}_i(s)) \\ \mathbf{\Phi}^{\mathrm{T}} &= (\mathbf{M}s^2 + \mathbf{C}s + \mathbf{K})^{-1}, \\ \mathbf{u}(t) &= \mathbf{H} \otimes \mathbf{p}(t), \qquad \hat{\mathbf{u}}(s) = \hat{\mathbf{H}}(s) \hat{\mathbf{p}}(s) \end{aligned} \tag{21}$$

where $\mathbf{M}$, $\mathbf{C}$ and $\mathbf{K}$ are the mass, damping and stiffness matrices of the system and $\otimes$ stands for the convolution operation. When the external excitation is a random process, the covariance of the response $\mathbf{u}$ can be represented as [24]

$$\begin{aligned} \mathbf{R}_{\mathrm{u}}(\tau) &= E(\mathbf{u}(t)\mathbf{u}(t+\tau)^{\mathrm{T}}) \\ &= E([\mathbf{H} \otimes \mathbf{p}](t)[\mathbf{H} \otimes \mathbf{p}](t+\tau)^{\mathrm{T}}) \\ &= [\mathbf{H} \oplus \mathbf{R}_p \otimes \mathbf{H}](\tau). \end{aligned} \tag{22}$$

Here $\oplus$ represents the cross-correlation between two signals and $\mathbf{R}_p(\tau)$ is the covariance matrix of input excitation. From the convolution theorem, the Fourier transform of the response covariance matrix, also known as the response power spectral density, is related to the excitation power spectral density through equation (23):

$$\begin{aligned} \therefore \hat{\mathbf{R}}_{\mathrm{u}}(\mathrm{i}\omega) &= \hat{\mathbf{H}}^*(\mathrm{i}\omega) \hat{\mathbf{R}}_p(\mathrm{i}\omega) \hat{\mathbf{H}}(\mathrm{i}\omega) \\ &= \mathbf{\Phi} \mathrm{diag}\,(\hat{h}_i(\mathrm{i}\omega))^* \mathbf{\Phi}^{\mathrm{T}} \hat{\mathbf{R}}_p(\mathrm{i}\omega) \\ &\quad \times \mathbf{\Phi} \mathrm{diag}\,(\hat{h}_i(\mathrm{i}\omega)) \mathbf{\Phi}^{\mathrm{T}}. \end{aligned} \tag{23}$$

In the case of white noise excitation, the ACF between displacement responses at node i and node j is obtained by taking the inverse Laplace transform of equation (23) (the same result can be achieved through performing time domain convolution/correlation in equation (22)):

$$\begin{aligned} \mathbf{R}_{\mathrm{u}}(\tau)_{\{i,j\}} &= \sum_{r=1}^{N} \frac{\phi_i^r}{m_r \omega_{\mathrm{D}r}} \sum_{\mathrm{s}=1}^{N} \sum_{k=1}^{N} \sum_{l=1}^{N} \beta_{jkl}^{rs} (J_{rs}^2 + I_{rs}^2)^{-\frac{1}{2}} \\ &\quad \times \exp(-\zeta_r \omega_{nr} \tau) \sin(\omega_{\mathrm{D}r} \tau + \gamma^{rs}), \\ \beta_{jkl}^{rs} &= \frac{\mathbf{R}_p(0)_{\{k,l\}} \phi_k^r \phi_j^{\mathrm{s}} \phi_l^{\mathrm{s}}}{m_{\mathrm{s}}}, \\ I_{rs} &= 2\omega_{\mathrm{D}r}(\zeta_r \omega_{nr} + \zeta_{\mathrm{s}} \omega_{ns}), \\ J_{rs} &= (\omega_{\mathrm{D}s}^2 - \omega_{\mathrm{D}r}^2) + (\zeta_r \omega_{nr} + \zeta_{\mathrm{s}} \omega_{ns})^2, \\ \tan \gamma_{rs} &= \frac{I_{rs}}{J_{rs}} \end{aligned} \tag{24}$$

where $(\cdot)_{\{k,l\}}$ refers to the term in the kth row and lth column of the subscripted matrix and ϕ_i^r is the ith component of mode shape r. This formulation is very similar to that given by [26]; only that an additional dimension of summation is introduced to account for possible spatial correlation among inputs at system DOFs. The ACF of acceleration measurements can be obtained by taking the fourth derivative of equation (24) and adding an impulse term to the expression

$$\mathbf{R}_{\ddot{u}}(\tau)_{\{i,j\}} = E(\mathbf{H}'(\mathbf{0})\mathbf{p}(\mathbf{t})\mathbf{p}(\mathbf{t})^{\mathrm{T}}\mathbf{H}'(\mathbf{0}))_{\{i,j\}} + \frac{\mathrm{d}^4[\mathbf{R}_{\mathrm{u}}(\tau)_{\{i,j\}}]}{\mathrm{d}\tau^4}$$

$$
\begin{aligned}
&= \Phi\Phi^{\mathrm{T}}\mathbf{R}_{\mathbf{p}}\Phi\Phi^{\mathrm{T}}_{\{i,j\}} \\
&+ \sum_{r=1}^{N}\frac{\phi_i^r}{m_r\omega_d^r}\sum_{s=1}^{N}\sum_{k=1}^{N}\sum_{l=1}^{N}\beta_{jkl}^{rs}(J_{rs}^2 \\
&+ I_{rs}^2)^{-\frac{1}{2}}\omega_{nr}^4\exp(-\zeta_r\omega_{\mathrm{n}}^r\tau) \\
&\times\{[(1-7\zeta_r^2)(1-\zeta_r^2)+\zeta_r^4]\sin(\omega_{\mathrm{D}r}\tau \\
&+ \gamma_{rs}) + 4\zeta_r(1-2\zeta_r^2)(1-\zeta_r^2)^{\frac{1}{2}} \\
&\times \cos(\omega_{\mathrm{D}r}\tau+\gamma_{rs})\}. \qquad (25)
\end{aligned}
$$

Given the sensitivity of the modal properties to structural damage (derived in section 3.2), sensitivity of the acceleration ACF to structural damage can be readily obtained:

$$
\begin{aligned}
\mathrm{d}\mathbf{R}_{\ddot{u}}(\tau)_{\{i,j\}} &= \sum_{l=1}^{N}\frac{\mathrm{d}\mathbf{R}_{\ddot{u}}(\tau)_{\{i,j\}}}{\mathrm{d}\omega_{\mathrm{n}l}}\,\mathrm{d}\omega_{\mathrm{n}l} \\
&+ \sum_{k=1}^{N}\sum_{l=1}^{N}\frac{\mathrm{d}\mathbf{R}_{\ddot{u}}(\tau)_{\{i,j\}}}{\mathrm{d}\phi_k^l}\,\mathrm{d}\phi_k^l. \qquad (26)
\end{aligned}
$$

The complete time domain sensitivity formula is too long, but sensitivities for the spectral density can be obtained as

$$
\begin{aligned}
\therefore \Delta\hat{\mathbf{R}}_{\mathrm{u}}(\mathrm{i}\omega) &= \Delta\{\hat{\mathbf{H}}^*(\mathrm{i}\omega)\hat{\mathbf{R}}_p(\mathrm{i}\omega)\hat{\mathbf{H}}(\mathrm{i}\omega)\} \\
&= -\hat{\mathbf{H}}^*(\mathrm{i}\omega)\Delta\mathbf{K}\hat{\mathbf{H}}^*(\mathrm{i}\omega)\hat{\mathbf{R}}_p(\mathrm{i}\omega)\hat{\mathbf{H}}(\mathrm{i}\omega) \\
&- \hat{\mathbf{H}}^*(\mathrm{i}\omega)\hat{\mathbf{R}}_p(\mathrm{i}\omega)\hat{\mathbf{H}}(\mathrm{i}\omega)\Delta\mathbf{K}\hat{\mathbf{H}}(\mathrm{i}\omega). \qquad (27)
\end{aligned}
$$

Because the Yule–Walker method is a time domain estimation method, the spectral density sensitivity will not be used for evaluation of the sensitivities of damage features. Still, this result is worth mentioning here as it provides a straightforward representation of the change in response ACF as a function of the global stiffness variation.

3.2. Sensitivity of system eigenvalues and eigenvectors with respect to changes in global stiffness matrix

To calculate the sensitivity of the ACF function to stiffness changes in the time domain, the sensitivity expressions for the natural frequencies and mode shapes are needed. In this section the first-order sensitivities of modal properties with respect to a change in the global stiffness matrix are presented.

To begin with, the classical structural dynamics equation is examined:

$$
\mathbf{M}\ddot{\mathbf{y}}(t)+\mathbf{C}\dot{\mathbf{y}}(t)+\mathbf{K}\mathbf{y}(t)=\mathbf{x}(t) \qquad (28)
$$

where $\mathbf{x}(t)$ and $\mathbf{y}(t)$ represent the continuous excitation input and displacement response, respectively. Natural vibration frequencies and mode shapes are obtained through eigenvalue analysis of the $\mathbf{M}$ and $\mathbf{K}$ matrices:

$$
(\mathbf{K}-\lambda_i\mathbf{M})\phi_i=0, \qquad \text{where } \lambda_i=\omega_i^2. \qquad (29)
$$

Here the λ_i and ϕ_i terms are the system eigenvalues and eigenvectors. Natural modal frequencies (angular) ω_i are the square roots of the corresponding eigenvalues. To get the sensitivity of the modal properties to changes in the stiffness matrix, first-order difference terms of both sides of equation (29) are calculated:

$$
\begin{aligned}
\Delta[(\mathbf{K}-\lambda_i\mathbf{M})\phi_i] &= \Delta\mathbf{K}\phi_i-\Delta\lambda_i\mathbf{M}\phi_i \\
&+ (\mathbf{K}-\lambda_i\mathbf{M})\Delta\phi_i=0, \qquad (30) \\
(\mathbf{K}-\lambda_i\mathbf{M})\Delta\phi_i &= \Delta\lambda_i\mathbf{M}\phi_i-\Delta\mathbf{K}\phi_i.
\end{aligned}
$$

Next all the eigenvectors are normalized with respect to the mass matrix and the changes in eigenvectors are expressed as a weighted sum of the original normalized eigenvectors:

$$
\Delta\phi_i=\sum_{k=1}^{N}d_{ik}\phi_k, \qquad \text{where } \phi_k^{\mathrm{T}}\mathbf{M}\phi_k=1. \qquad (31)
$$

Both sides of equation (31) are then premultiplied with $\phi_r^{\mathrm{T}}(r\neq i)$ and the mass/stiffness orthogonality between different modes is utilized to get the respective weight for each eigenvector:

$$
\begin{aligned}
\Delta\lambda_i\phi_r^{\mathrm{T}}\mathbf{M}\phi_i-\phi_r^{\mathrm{T}}\Delta\mathbf{K}\phi_i &= -\phi_r^{\mathrm{T}}\Delta\mathbf{K}\phi_i, \\
\sum_{k=1}^{N}d_{ik}\phi_r^{\mathrm{T}}(\mathbf{K}-\lambda_i\mathbf{M})\phi_k &= d_{ir}\phi_r^{\mathrm{T}}(\mathbf{K}-\lambda_i\mathbf{M})\phi_r \\
&= d_{ir}(\phi_r^{\mathrm{T}}\mathbf{K}\phi_r-\lambda_i\phi_r^{\mathrm{T}}\mathbf{M}\phi_r) \\
&= d_{ir}(\lambda_r-\lambda_i), \\
d_{ir}(\lambda_r-\lambda_i) &= -\phi_r^{\mathrm{T}}\Delta\mathbf{K}\phi_i \\
\Rightarrow d_{ir} &= -\frac{\phi_r^{\mathrm{T}}\Delta\mathbf{K}\phi_i}{\lambda_r-\lambda_i}.
\end{aligned} \qquad (32)
$$

When $r=i$, it can be proved that $d_{ir}=0$. Therefore, the sensitivity of the ith eigenvector is orthogonal to itself and is computed as equation (33):

$$
\begin{aligned}
\Delta(\phi_i^{\mathrm{T}}\mathbf{M}\phi_i) &= 1\Rightarrow\Delta\phi_i^{\mathrm{T}}\mathbf{M}\phi_i=0 \\
\Rightarrow d_{rr} &= \phi_i^{\mathrm{T}}\mathbf{M}\Delta\phi_i/\phi_i^{\mathrm{T}}\mathbf{M}\phi_i=0, \\
\therefore\Delta\phi_i &= \sum_{\substack{r=1\\ r\neq i}}^{N}-\frac{\phi_r^{\mathrm{T}}\Delta\mathbf{K}\phi_i}{\lambda_r-\lambda_i}\phi_r.
\end{aligned} \qquad (33)
$$

The sensitivity of the natural frequencies is obtained by premultiplying both sides of equation (31) with ϕ_i^{T}:

$$
\begin{aligned}
\phi_i^{\mathrm{T}}(\mathbf{K}-\lambda_i\mathbf{M})\Delta\phi_i &= \Delta\lambda_i\phi_i^{\mathrm{T}}\mathbf{M}\phi_i-\phi_i^{\mathrm{T}}\Delta\mathbf{K}\phi_i \\
\Rightarrow\Delta\lambda_i &= \phi_i^{\mathrm{T}}\Delta\mathbf{K}\phi_i, \\
\because\lambda_i &= \omega_i^2, \qquad \therefore\Delta\omega_i=\frac{\phi_i^{\mathrm{T}}\Delta\mathbf{K}\phi_i}{2\omega_i}.
\end{aligned} \qquad (34)
$$

Sensitivity of the signal ACF to stiffness change can be calculated by substituting equations (33) and (34) into (26). Thus to obtain the damage sensitivity of the features, only their sensitivity with respect to the acceleration ACF is needed.

3.3. Sensitivity of the AR coefficients/spectra to ACF values

From equation (11), the sensitivity of the Yule–Walker AR estimators with respect to the changes in ACF can be derived

as

$$\mathrm{d}\begin{bmatrix}\hat{\varphi}_1\\ \hat{\varphi}_2\\ \hat{\varphi}_3\\ \vdots\\ \hat{\varphi}_p\end{bmatrix} \Big/ \mathrm{d}R(\tau) = \begin{cases} -\boldsymbol{\Gamma}^{-2}\boldsymbol{\gamma}, & \tau = 0 \\ \boldsymbol{\Gamma}^{-1}\mathbf{e}_\tau - \boldsymbol{\Gamma}^{-1}\ \text{toeplitz}\,(\mathbf{e}_{\tau+1})\boldsymbol{\Gamma}^{-1}\boldsymbol{\gamma} & 1 < \tau < p, \\ \boldsymbol{\Gamma}^{-1}\mathbf{e}_p, & \tau = p \end{cases} \tag{35}$$

where $\mathbf{e}_\tau$ is a $(p \times 1)$ column vector with all elements equal to zero except for element τ, which equals 1. For the AR spectrum, the definition here states that it is

$$\hat{S}_{\mathrm{AR}}^{(p)}(\omega) = \frac{1}{|\hat{\varphi}(\mathrm{e}^{\mathrm{j}\omega})|^2} = \frac{1}{\left|\sum_{k=0}^{p}\hat{\varphi}_k \mathrm{e}^{-\mathrm{j}\omega k}\right|^2}. \tag{36}$$

In this definition, $\hat{\varphi}_0 = 1$. Its sensitivity to changes in coefficients can be computed as

$$\begin{aligned} \frac{\mathrm{d}\hat{S}_{\mathrm{AR}}^{(p)}(\omega)^{-1}}{\mathrm{d}\hat{\varphi}_k} &= 2\,\mathrm{Re}\left\{\mathrm{e}^{-\mathrm{j}\omega k}\left(\sum_{n=0}^{p}\hat{\varphi}_n \mathrm{e}^{\mathrm{j}\omega n}\right)\right\}, \\ \frac{\mathrm{d}\hat{S}_{\mathrm{AR}}^{(p)}(\omega)}{\mathrm{d}\hat{\varphi}_k} &= -2\,\mathrm{Re}\left\{\mathrm{e}^{-\mathrm{j}\omega k}\left(\sum_{n=0}^{p}\hat{\varphi}_n \mathrm{e}^{\mathrm{j}\omega n}\right)\right\}\hat{S}_{\mathrm{AR}}^{(p)}(\omega)^2. \end{aligned} \tag{37}$$

Thus by combining equations (35) and (37) the sensitivity of the spectrum to ACF changes is calculated.

3.4. Sensitivity of the AR coefficients/spectra to the increase in the noise level

To compute the influence of noise on damage feature estimation, consider the signal covariance sequence of contaminated signals. When white noise of standard deviation σ is added to the signal, its ACF sequence R_{c} will be

$$R_{\mathrm{c}}(\tau) = R(\tau) + R_{\mathrm{n}}(\tau) = R(\tau) + \sigma^2\delta(\tau), \tag{38}$$

where $R_{\mathrm{n}}(\tau)$ denotes the ACF of white noise. Therefore, the sensitivity of the estimated coefficients to the variance of additive Gaussian noise will be

$$\frac{\mathrm{d}[\hat{\varphi}_1, \hat{\varphi}_2, \ldots, \hat{\varphi}_p]^{\mathrm{T}}}{\mathrm{d}\sigma^2} = \frac{\mathrm{d}[(\boldsymbol{\Gamma} + \sigma^2\mathbf{I})^{-1}\boldsymbol{\gamma}]}{\mathrm{d}\sigma^2} = -\boldsymbol{\Gamma}^{-2}\boldsymbol{\gamma}. \tag{39}$$

Sensitivity of the AR spectrum to the noise level can be derived through combining equations (39) and (37) in section 3.3. It should be noted that the above formula only accounts for the extreme case (i.e. number of samples $N_{\mathrm{s}} = \infty$). For the finite sample scenario, the estimated noise correlation $\hat{\rho}_{\mathrm{n}}(\tau)$ is asymptotically normally distributed with variance n^{-1} at nonzero lags [11]. As such,

$$\begin{aligned} \frac{\mathrm{d}[\hat{\varphi}_1, \hat{\varphi}_2, \ldots, \hat{\varphi}_p]^{\mathrm{T}}}{\mathrm{d}\sigma^2} &= -\boldsymbol{\Gamma}^{-1} \\ &\times \begin{bmatrix} 1 & \hat{\rho}_{\mathrm{n}}(1) & \hat{\rho}_{\mathrm{n}}(2) & \cdots & \hat{\rho}_{\mathrm{n}}(p-1) \\ \hat{\rho}_{\mathrm{n}}(1) & 1 & \hat{\rho}_{\mathrm{n}}(1) & \cdots & \hat{\rho}_{\mathrm{n}}(p-2) \\ \hat{\rho}_{\mathrm{n}}(2) & \hat{\rho}_{\mathrm{n}}(1) & 1 & \cdots & \hat{\rho}_{\mathrm{n}}(p-3) \\ \vdots & \vdots & \vdots & \ddots & \vdots \\ \hat{\rho}_{\mathrm{n}}(p-1) & \hat{\rho}_{\mathrm{n}}(p-2) & \hat{\rho}_{\mathrm{n}}(p-3) & \cdots & 1 \end{bmatrix}\boldsymbol{\Gamma}^{-1} \\ &\times \begin{bmatrix} R(1) \\ R(2) \\ R(3) \\ \vdots \\ R(p) \end{bmatrix}. \end{aligned} \tag{40}$$

The ACF of the original signal is also affected by estimation errors and exhibits an asymptotic Gaussian distribution [11]. To avoid including unnecessary statistical complexities and focus on the direct influence of structural damage/measurement noise level on damage features here it is assumed that the ACF estimators are exact (the asymptotic case).

3.5. Sensitivity of the distance measures to changes in AR coefficients/spectra

The theoretical feature values under the null hypothesis will be needed for evaluation of relative sensitivity. The AR coefficient estimators are asymptotically unbiased and follow a multivariate Gaussian distribution with covariance matrix $\frac{\sigma_{\mathrm{e}}^2}{N}\boldsymbol{\Gamma}^{-1}(\sigma_{\mathrm{e}}^2 = R(0) - \boldsymbol{\gamma}^{\mathrm{T}}\boldsymbol{\Gamma}^{-1}\boldsymbol{\gamma})$ [11]. Under this assumption, the Mahalanobis distance feature for the undamaged structural state has a chi-squared distribution with p degrees-of-freedom, and its statistical expectation is p. The expression for the expected value of the Mahalanobis distance for the general case is presented in equation (41):

$$\begin{aligned} E(D^2) &= E(\boldsymbol{\varphi}_{\mathrm{u}}^{\mathrm{T}} - \bar{\boldsymbol{\varphi}}_{\mathrm{b}}^{\mathrm{T}})\boldsymbol{\Sigma}_{\mathrm{b}}^{-1}(\boldsymbol{\varphi}_{\mathrm{u}} - \bar{\boldsymbol{\varphi}}_{\mathrm{b}}) \\ &= E[(\boldsymbol{\varphi}_{\mathrm{u}}^{\mathrm{T}} - \bar{\boldsymbol{\varphi}}_{\mathrm{u}}^{\mathrm{T}})\boldsymbol{\Sigma}_{\mathrm{b}}^{-1}(\boldsymbol{\varphi}_{\mathrm{u}} - \bar{\boldsymbol{\varphi}}_{\mathrm{u}})] \\ &\quad + [(\bar{\boldsymbol{\varphi}}_{\mathrm{u}}^{\mathrm{T}} - \bar{\boldsymbol{\varphi}}_{\mathrm{b}}^{\mathrm{T}})\boldsymbol{\Sigma}_{\mathrm{b}}^{-1}(\bar{\boldsymbol{\varphi}}_{\mathrm{u}} - \bar{\boldsymbol{\varphi}}_{\mathrm{b}})] \\ &= \mathrm{trace}\,[\boldsymbol{\Sigma}_{\mathrm{b}}^{-1}\boldsymbol{\Sigma}_{\mathrm{u}}] + [(\bar{\boldsymbol{\varphi}}_{\mathrm{u}}^{\mathrm{T}} - \bar{\boldsymbol{\varphi}}_{\mathrm{b}}^{\mathrm{T}})\boldsymbol{\Sigma}_{\mathrm{b}}^{-1}(\bar{\boldsymbol{\varphi}}_{\mathrm{u}} - \bar{\boldsymbol{\varphi}}_{\mathrm{b}})]. \end{aligned} \tag{41}$$

The first- and second-order sensitivities of $E(D^2)$ to signal covariance can then be computed. Note that, for notational simplicity, θ is used to express the ACF value at an arbitrary lag:

$$\left.\frac{\mathrm{d}E(D^2)}{\mathrm{d}\theta}\right|_{\boldsymbol{\varphi}_{\mathrm{u}}=\boldsymbol{\varphi}_{\mathrm{b}},\,\boldsymbol{\Sigma}_{\mathrm{u}}=\boldsymbol{\Sigma}_{\mathrm{b}}} = \mathrm{trace}\left[\boldsymbol{\Sigma}_{\mathrm{b}}^{-1}\frac{\mathrm{d}\boldsymbol{\Sigma}_{\mathrm{u}}}{\mathrm{d}\theta}\right], \tag{42}$$

$$\begin{aligned} \left.\frac{\mathrm{d}^2E(D^2)}{\mathrm{d}\theta^2}\right|_{\boldsymbol{\varphi}_{\mathrm{u}}=\boldsymbol{\varphi}_{\mathrm{b}},\,\boldsymbol{\Sigma}_{\mathrm{u}}=\boldsymbol{\Sigma}_{\mathrm{b}}} &= \mathrm{trace}\left[\boldsymbol{\Sigma}_{\mathrm{b}}^{-1}\frac{\mathrm{d}^2\boldsymbol{\Sigma}_{\mathrm{u}}}{\mathrm{d}\theta^2}\right] \\ &\quad + 2\left[\frac{\mathrm{d}(\bar{\boldsymbol{\varphi}}_{\mathrm{u}}^{\mathrm{T}} - \bar{\boldsymbol{\varphi}}_{\mathrm{b}}^{\mathrm{T}})}{\mathrm{d}\theta}\boldsymbol{\Sigma}_{\mathrm{b}}^{-1}\frac{\mathrm{d}(\bar{\boldsymbol{\varphi}}_{\mathrm{u}} - \bar{\boldsymbol{\varphi}}_{\mathrm{b}})}{\mathrm{d}\theta}\right]. \end{aligned} \tag{43}$$

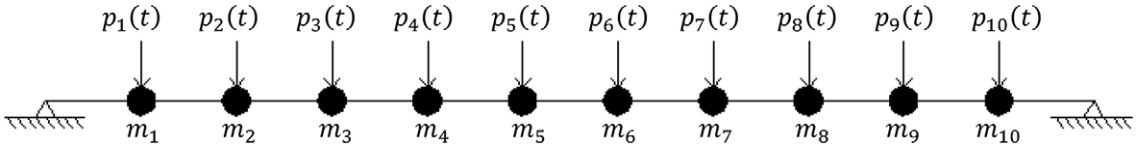

Figure 4. The simulated 10-DOF model.

The expressions for the first- and second-order sensitivity of $\boldsymbol{\Sigma}_u$ with respect to signal ACF are presented in appendix A; the contribution of these terms to the feature value is relatively small compared to the mean shift in the application described in section 4.

Under the Gaussian assumption, the AR spectral estimates also asymptotically follow a normal distribution; as p^3/N decreases, $\sqrt{\frac{N}{p}}(\bar{S}_b - S)/\bar{S}_b$ converges to a normal distribution with asymptotic variance equal to 4 at DC and 2 otherwise [27]. Therefore the expected value for the Cosh distance of the baseline state can be written as the sum of moments of this Gaussian distribution:

$$E(C)|_{ES(\omega_j)=\bar{S}_b(\omega_j)} = \frac{1}{2N}\sum_{j=1}^{N} E\left[\frac{S(\omega_j)}{\bar{S}_b(\omega_j)} + \frac{\bar{S}_b(\omega_j)}{S(\omega_j)} - 2\right]$$
$$= \frac{1}{2N}\sum_{j=1}^{N} E\left[\frac{\bar{S}_b(\omega_j)}{S(\omega_j)} - 1\right]$$
$$= \frac{1}{2N}\sum_{j=1}^{N} E\left[\frac{1}{(S(\omega_j) - \bar{S}_b(\omega_j))/\bar{S}_b(\omega_j) + 1} - 1\right].$$

The following is obtained after performing a geometric series expansion on $(S(\omega_j) - \bar{S}_b(\omega_j))/\bar{S}_b(\omega_j)$ for the equation above:

$$E(C)|_{ES(\omega_j)=\bar{S}_b(\omega_j)} \frac{1}{2N}\sum_{j=1}^{N} E\left[\sum_{l=1}^{\infty}\left(\frac{S(\omega_j) - \bar{S}_b(\omega_j)}{\bar{S}_b(\omega_j)}\right)^{2l}\right]. \quad (44)$$

Since the normal assumption is valid only in the asymptotic sense, and higher-order statistical moments are less significant in value and affected more by the deviation from this assumption, only the first two terms ($l = 1, 2$) will be considered in applications in this paper.

The sensitivity expressions of Cosh distance are obtained in a similar manner as that for Mahalanobis distance:

$$\frac{dE(C)}{d\theta}\bigg|_{ES(\omega_j)=\bar{S}_b(\omega_j)}$$
$$= \frac{1}{2N}\sum_{1}^{N}\left\{\frac{dES(\omega_j)}{d\theta}\frac{1}{\bar{S}_b(\omega_j)} + \frac{dE[S(\omega_j)^{-1}]}{d\theta}\bar{S}_b(\omega_j)\right\}$$
$$= \frac{1}{2N}\sum_{1}^{N}\left\{\frac{dES(\omega_j)}{d\theta}\frac{1}{\bar{S}_b(\omega_j)} + \frac{d\sum_{l=0}^{\infty} E(\frac{\bar{S}_b(\omega_j)-S(\omega_j)}{\bar{S}_b(\omega_j)})^l}{d\theta}\right\} = 0, \quad (45)$$

$$\frac{d^2E(C)}{d\theta^2}\bigg|_{S(\omega_j)=\bar{S}_b(\omega_j)}$$
$$= \frac{1}{2N}\sum_{1}^{N}\left\{\frac{d^2ES(\omega_j)}{d\theta^2}\frac{1}{\bar{S}_b(\omega_j)} + \frac{d^2\sum_{l=0}^{\infty} E(\frac{\bar{S}_b(\omega_j)-S(\omega_j)}{\bar{S}_b(\omega_j)})^l}{d\theta^2}\right\}$$
$$= \frac{1}{2N}\sum_{1}^{N}\left(\frac{dS(\omega_j)}{d\theta}\right)^2\frac{2}{\bar{S}_b(\omega_j)^2}. \quad (46)$$

The damage/noise sensitivities of both features are found as the product of the sensitivities of features to ACF and the sensitivities of ACF to structural damage/measurement noise.

4. Simulation example: sensitivity analysis for a 10-DOF structure

To verify the sensitivity analysis scheme presented in section 3, it is applied to a 10-DOF model with linear topology and simply supported at both ends (figure 4). The mass of each node is 2 tons, the length of each element is 25 m and the section stiffness (EI) is 2.5×10^5 kN m^2. Damage is defined as a stiffness reduction in the inter-node elements and a procedure to transform the local section stiffness change (ΔEI) to a global stiffness change ($\Delta\mathbf{K}$) is developed in appendix B.

Spatially and chronologically uncorrelated random excitation is applied at each node of the system. Acceleration signals are simulated from the system using Newmark's method and both feature values are extracted from the signals during multiple runs of the simulation. Each simulation returns a group of Cosh distance values and a group of Mahalanobis distance values, and feature mean and confidence interval can be henceforth obtained. Pooling results from all runs of the simulation the average and confidence interval of means from respective feature groups can be calculated. These simulation results regarding the effects of local damage/measurement noise on feature values are compared with theoretical analysis results and sensitivity analysis results. Here theoretical results refer to those computed directly from the theoretical ACF (equations (25) and (38)) for each damage/measurement noise case and sensitivity results are those obtained from concatenating sensitivity expressions derived step-by-step in section 3. For all simulations and computations, the AR model order is set at 20. During each run of the simulation, 88 signal

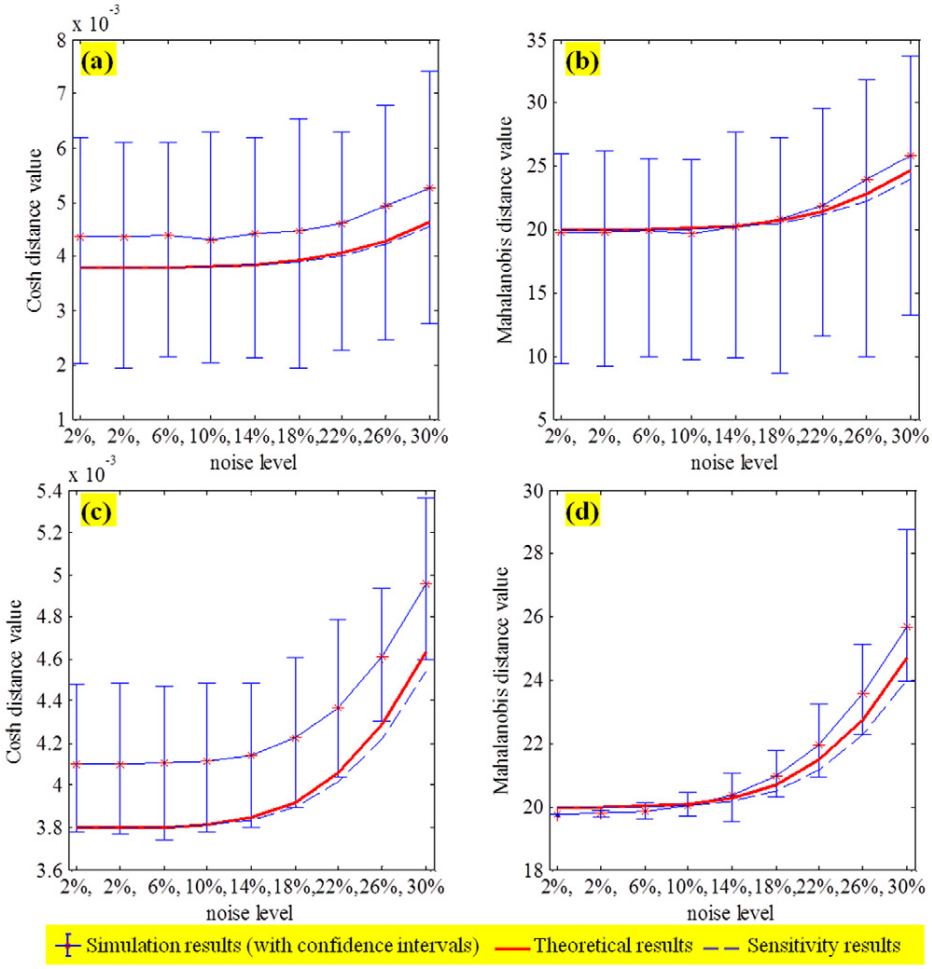

Figure 5. Plots of the Mahalanobis distance and Cosh distance damage feature values as noise level increases. Plots (a) and (b) show simulation results from one experiment, (c) and (d) show the average simulation results from 50 runs (confidence intervals are constructed based on average values).

segments, each containing 5400 data points sampled at a frequency of 50 Hz, are used to calculate the Mahalanobis distance and Cosh distance features. Two figures are created to contrast the results, which are from calculations performed for acceleration signals from node 4. For all the plots within each figure, the star-marked solid line with 95% confidence intervals, the dashed line and the thick solid line represent the results from simulation, sensitivity analysis and theoretical analysis, respectively.

Figure 5 shows the trends of Mahalanobis distance and Cosh distance as the noise level increases. Signals with 2% noise level are used as the baseline and another case with 2% noise level is included for false positive testing [12, 17]. Because simulations that involve random vibration generation come with uncertainty (i.e. yield different results on each run), it is beneficial to include results from another set of signals collected under the same noise/structural state to demonstrate the variation, which provides a reference on the amount of variation that can be confidently identified by the features. Noise level in this paper is defined as the ratio between the standard deviation of measurement noise and that of the actual signal. In SHM practice both the noise and signal strength vary depending on the application; noise amplitude can be from tens to thousands μg and the sampled ambient vibration signal amplitude can be of the order of a few to hundreds mg [18, 28, 29]. Thus, the noise level values investigated here (2%–30%) fall in the range of expected noise levels. The three lines in the plots have relatively close values in comparison to the large confidence interval from one simulation, with the average relative deviation from the theoretical to sensitivity analysis results with respect to the confidence interval length at 1.31% and 0.68% for the Mahalanobis and Cosh distance features, respectively, and that from simulation mean to sensitivity analysis results at 4.02% and 14.22%. There is a noticeable difference between the simulation and theoretical analysis because the derivations are based on the asymptotic theory, which is but an approximation for large-sample-base estimation. The confidence bounds generated through simulation for both features indicate positive skew in distribution, a fact compatible with the assumptions on their respective asymptotic distribution. The average Cosh distance values from 50 simulations have a much reduced, yet still largely uniform, confidence interval (from $\pm$50% around the mean to $\pm$10% around the mean)

Table 1. Outlier percentages from simulation, theory and sensitivity analysis as noise level increases.

		Noise levels								
Feature type	Outlier percentage	**0.02**	**0.02**	**0.06**	**0.1**	**0.14**	**0.18**	**0.22**	**0.26**	**0.3**
C[a]	Simulation	0.05	0.05	0.05	0.07	0.08	0.06	0.04	0.11	0.12
	Theoretical	0.05	0.05	0.06	0.06	0.06	0.06	0.08	0.08	0.1
	Sensitivity	0.06	0.06	0.06	0.06	0.06	0.06	0.06	0.08	0.09
D^2[b]	Simulation	0.05	0.05	0.05	0.06	0.07	0.08	0.09	0.13	0.21
	Theoretical	0.05	0.05	0.06	0.06	0.06	0.06	0.06	0.08	0.1
	Sensitivity	0.06	0.06	0.06	0.06	0.06	0.06	0.06	0.07	0.09

[a] C—Cosh distance.
[b] D^2—Mahalanobis distance.

over different cases, while the confidence interval for average Mahalanobis distance values is expanding along the x axis. The simulation mean for the Cosh distance is 8% higher than the computed theoretical value, but their increasing tendency is almost parallel. The baseline value estimation for Mahalanobis distance is more precise than Cosh distance because the value for the latter is from a truncated series (equation (44)) and the sensitivity measure predicts the varying trend of Mahalanobis distance less exactly than that of Cosh distance because computation of the former uses the covariance matrix obtained from asymptotic theory, which adds in error. Sensitivity analysis values for both features start quite close to the theoretical results when deviation from the original/baseline state is small, yet their difference grows larger as the deviation increases because of higher-order effects that are neglected in the linearization step of sensitivity analysis. The sensitivity analysis in this case study underestimates the feature value for significant changes in structural state/signal noise level. Note here the distribution variance terms (trace$[\boldsymbol{\Sigma}_b^{-1}\frac{d\boldsymbol{\Sigma}_u}{d\theta}]$ and trace $[\boldsymbol{\Sigma}_b^{-1}\frac{d^2\boldsymbol{\Sigma}_u}{d\theta^2}]$) are not considered as the computation is complex and their relative influence is small.

In applications the two damage features studied are often employed in a statistical control style [12, 14, 17]. In other words, the features will be extracted in large quantities and the system is identified as changed when the number of feature values exceeding a pre-set threshold becomes significant (i.e. more than a certain proportion of the total number of feature samples). Table 1 shows the number of outliers from the simulation together with those predicted from theoretical and sensitivity analysis as the noise level increases. Here for each feature the threshold is set at the 5% significant level and determined empirically from the baseline feature population. Because the theoretical/sensitivity derivations involve only the mean shift of features, an assumption is made that the higher moments of the feature distributions do not change much over the different states. As such, outlier numbers can be predicted by adding the mean deviations from theoretical/sensitivity analysis to the original baseline feature values and then examining the number of outliers in the newly obtained feature group. Results from the table indicate that for the Cosh distance feature the theoretical/sensitivity approaches predict the outlier percentage change trend with good accuracy; the simulation results are fluctuating around the predictions. For the Mahalanobis distance feature the simulations produce higher outlier percentages than the other two options, because the dispersion of this feature noticeably increased as the noise level rises (figure 5). The sensitivity method gives a more conservative estimate on outlier percentage increases as noise level rises than the theoretical method for both damage features. Also, the outlier counts for the damage features do not vary significantly till the noise level reaches 22%–26%.

Figure 6 presents the trends of the two features as a stiffness reduction between node 4 and 5 grows. The stiffness loss is expressed as a percentage of the original element stiffness and measurements are assumed to contain 2% noise. The parabolic trends and relative positions of the lines are similar to those shown in figure 5. This observation is not very surprising as both noise and structural damage affect the feature values through the acceleration signal ACF. For both feature values, the 16% stiffness reduction produces about the same amount of mean shift as that done by an increase in noise level from 2% to a value between 26% and 30%. Since here the structure and a single type of damage are specified and excitation/noise characteristics are not varying, the feature values can directly reflect structural stiffness loss. In the general case, this is not feasible because the information based on which features are extracted is limited (i.e., single channel acceleration).

Table 2 contains the outlier ratios as obtained from the three approaches. The number of outliers in each feature from theory/sensitivity analysis follows a similar procedure as that used in table 1, where the baseline feature samples are involved in the computation. While the theoretical/sensitivity analysis predictions for Cosh distance agree with the simulation, those predictions for Mahalanobis distance are often well below the simulation value since the feature dispersion increases as damage grows more severely (figure 6). Again, the sensitivity method as a whole underestimates the outlier percentages at high damage levels because of the model error introduced by linearization, indicating that it produces a lower bound. Here the Mahalanobis distance responds to damage at an earlier level (i.e. 8% stiffness reduction corresponds to a 10% outlier percentage from the simulation), while the Cosh distance only yields a significant change at a later stage (i.e. 12% stiffness reduction corresponds to a 10% outlier percentage).

Please note that all sensitivity expressions here are derived for the general case, except for the sensitivity of the local section stiffness change (ΔEI) to global stiffness

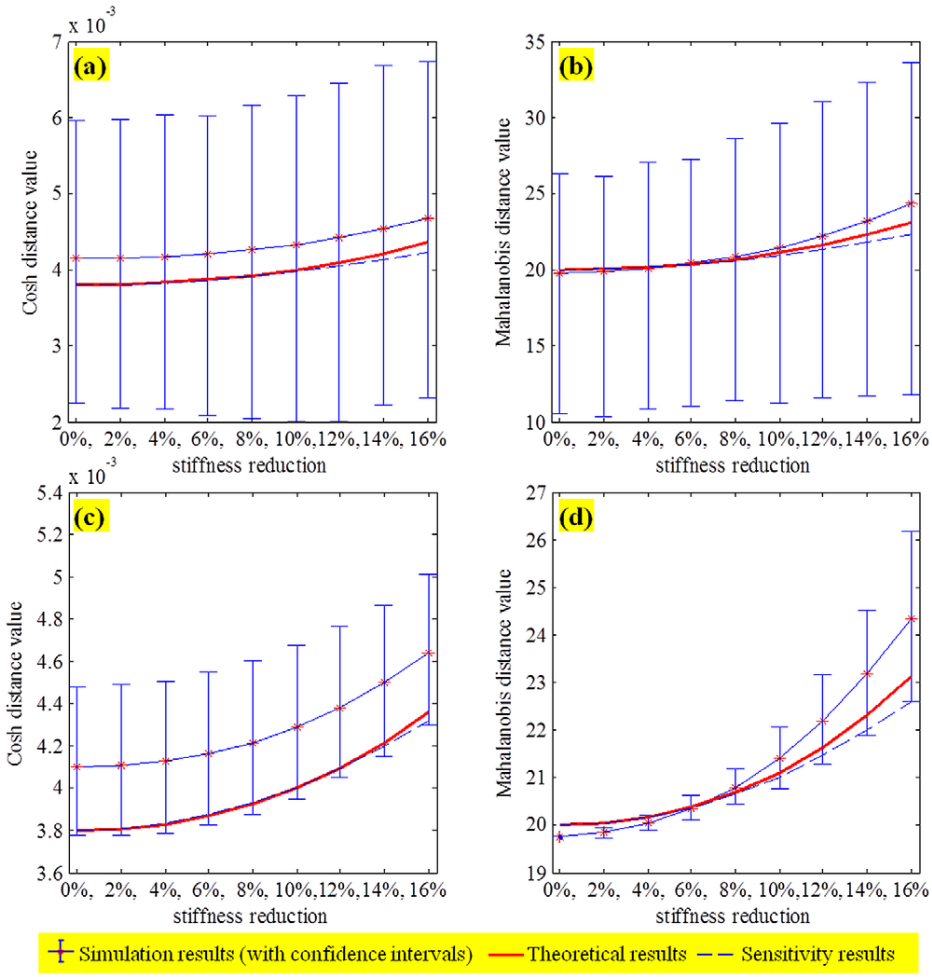

Figure 6. Plots of the damage feature values obtained as the stiffness of the element between 4 and 5 decreases. Plots (a) and (b) show simulation results from one experiment, while (c) and (d) show the average simulation results from 50 runs.

Table 2. Outlier percentages from simulation, theory and sensitivity analysis as damage level increases.

		Damage levels								
Feature type	Outlier percentage	**0**	**0.02**	**0.04**	**0.06**	**0.08**	**0.1**	**0.12**	**0.14**	**0.16**
C	Simulation	0.05	0.06	0.05	0.06	0.08	0.07	0.1	0.11	0.16
	Theoretical	0.05	0.06	0.07	0.08	0.09	0.1	0.11	0.13	0.13
	Sensitivity	0.05	0.06	0.07	0.07	0.09	0.09	0.11	0.12	0.13
D^2	Simulation	0.05	0.06	0.05	0.09	0.1	0.14	0.18	0.23	0.31
	Theoretical	0.05	0.06	0.06	0.06	0.06	0.06	0.08	0.1	0.14
	Sensitivity	0.05	0.06	0.06	0.06	0.06	0.06	0.06	0.08	0.1

change ($\Delta\mathbf{K}$), which is developed for this particular simulated structure. Results at other nodes also show agreement among curves from the three methods and, due to space limitations, are not presented here. Another observation worth mentioning for this case study is that, as the measurement location moves away from the damage location, the change in damage feature values becomes less significant. In fact, the damage features are hardly reporting any noticeable changes at the first and last node.

5. Conclusion and discussion

This paper proposes a sensitivity analysis approach to investigate the effect of measurement noise and structural damage on two existing damage features, the Mahalanobis distance of AR coefficients and the Cosh distance of AR model spectra. It is found that both feature values increase parabolically with respect to increases in local damage extent and measurement noise level. The approach is used to predict the feature values from a numerical 10-DOF bridge model in several damage/noise level cases, and the outcome is in good agreement with that from simulated acceleration signals and theoretical calculations. This observation supports the validity of the proposed approach, which is a more efficient way to examine the behavior (sensitivity and robustness) of damage features than repeating the simulation process for a number of times. The reason for that is because simulation requires

the generation of structural vibration signals and extraction of feature values for each noise/damage state, but the sensitivity values, once computed, can be applied to multiple states.

Since the approach introduced here involves using a structural FE model, modeling error can affect the procedure from two aspects: the baseline state signal estimation, which affects the noise and damage sensitivity estimation, and the relation between the structural measurements and local damage, which affects the damage sensitivity. For the first part of the problem, civil structures under ambient vibration are generally only well excited in a few low frequency modes. If the FE model can be tuned such that its modes match those measured from the real structure at the original state, then the structural baseline state response ACFs can be estimated from the FE model with good accuracy. For the second part, there is no definite solution. However, ranges in which FE parameters vary can be assumed and damage sensitivity expressions for certain parameter sets within the range can be computed to obtain the lower/upper bounds of damage feature sensitivity.

It is noted that the Mahalanobis distance and Cosh distance features respond not only to structural damage but also to increase in the noise level. This fact implies that both features are not completely robust to variations unrelated to structural change. This is partially due to the fact that the damage identification algorithms use only the response from a single channel, which is generated as a result of the interaction between several components (structure, environment and excitation). However, as shown in the simulation example above, it takes a significant increase in the noise level to produce a feature value change that matches that from a moderate reduction of stiffness for both AR features. Thus, these damage indices are effective in monitoring a structure with reasonably stable operating conditions.

The variation of environmental conditions (temperature, humidity, etc) often affects the damage features through their influence on the structural material properties (and hence the stiffness properties). The traffic variation will change the excitation amplitude, spatial pattern and frequency contents. AR-based features will be robust to the excitation amplitude but are affected by the other two excitation factors. These non-structural influences are not examined in an analytical manner unless the functional relationship between the environmental conditions and structural stiffness is known and the form of excitation variation is defined. The sensitivity terms can be derived by taking the derivative of signal ACF with respect to these sources of influence. Further research is needed to address these issues.

Acknowledgments

The research described in this paper is supported by the National Science Foundation through Grant No. CMMI-0926898 by the Sensors and Sensing Systems Program and by a grant from the Commonwealth of Pennsylvania, Department of Community and Economic Development, through the Pennsylvania Infrastructure Technology Alliance (PITA).

Appendix A. Calculation of the first- and second-order derivative of the covariance matrix of AR coefficient vectors with respect to the ACF

The first-order derivative of the covariance matrix of the unknown state AR coefficients is first expressed as a function of the derivatives of the AR residual variance σ_e and that of the inverse of the ACF Toeplitz matrix $\mathbf{\Gamma}$:

$$\frac{d\Sigma_u}{dR(\tau)} = \frac{d\sigma_e}{dR(\tau)}\mathbf{\Gamma}^{-1} + \sigma_e\frac{d\mathbf{\Gamma}^{-1}}{dR(\tau)}. \tag{A.1}$$

According to their respective definitions, specific expressions for $\frac{d\sigma_e}{dR(\tau)}$ and $\frac{d\mathbf{\Gamma}^{-1}}{dR(\tau)}$ are derived as follows:

$$\frac{d\sigma_e}{dR(\tau)} = \begin{cases} 1 + \boldsymbol{\gamma}^T\mathbf{\Gamma}^{-1}\mathbf{\Gamma}^{-1}\boldsymbol{\gamma}, & \tau = 0 \\ \boldsymbol{\gamma}^T\mathbf{\Gamma}^{-1}\ \text{toeplitz}\,(\mathbf{e}_{\tau+1})\mathbf{\Gamma}^{-1}\boldsymbol{\gamma} - 2\mathbf{e}_\tau^T\mathbf{\Gamma}^{-1}\boldsymbol{\gamma}, & \\ & 1 \le \tau \le p-1 \\ -2\mathbf{e}_\tau^T\mathbf{\Gamma}^{-1}\boldsymbol{\gamma}, & \tau = p \end{cases} \tag{A.2}$$

$$\frac{d\mathbf{\Gamma}^{-1}}{dR(\tau)} = \begin{cases} -\mathbf{\Gamma}^{-1}\ \text{toeplitz}\,(e_{\tau+1})\mathbf{\Gamma}^{-1}, & 0 \le \tau \le p-1 \\ \mathbf{0}, & \tau = p. \end{cases} \tag{A.3}$$

Likewise the second-order derivative of Σ_u can be obtained as a function of the first-/second-order derivatives of σ_e and $\mathbf{\Gamma}^{-1}$:

$$\frac{d^2\Sigma_u}{dR(\tau)^2} = \frac{d^2\sigma_e}{dR(\tau)^2}\mathbf{\Gamma}^{-1} + 2\,\frac{d\sigma_e}{dR(\tau)}\frac{d\mathbf{\Gamma}^{-1}}{dR(\tau)} + \sigma_e\,\frac{d^2\mathbf{\Gamma}^{-1}}{dR(\tau)^2}. \tag{A.4}$$

The second-order derivatives of σ_e and $\mathbf{\Gamma}^{-1}$ are computed by taking the derivatives of equations (A.2) and (A.3). Note that application of these formulas requires substituting in values of the first-order derivative of $\mathbf{\Gamma}^{-1}$:

$$\frac{d^2\sigma_e}{dR(\tau)^2} = \begin{cases} 2\boldsymbol{\gamma}^T\dfrac{d\mathbf{\Gamma}^{-1}}{dR(0)}\mathbf{\Gamma}^{-1}\boldsymbol{\gamma}, & \tau = 0 \\ 2\boldsymbol{\gamma}^T\dfrac{d\mathbf{\Gamma}^{-1}}{dR(\tau)}\ \text{toeplitz}\,(\mathbf{e}_{\tau+1})\mathbf{\Gamma}^{-1}\boldsymbol{\gamma} & \\ \quad - 2\boldsymbol{\gamma}^T\dfrac{d\mathbf{\Gamma}^{-1}}{dR(\tau)}\mathbf{e}_\tau - 2\mathbf{e}_\tau^T\dfrac{d\mathbf{\Gamma}^{-1}}{dR(\tau)}\boldsymbol{\gamma} & \\ \quad - 2\mathbf{e}_\tau^T\mathbf{\Gamma}^{-1}\mathbf{e}_\tau, & 1 \le \tau \le p-1 \\ -2\mathbf{e}_p^T\mathbf{\Gamma}^{-1}\mathbf{e}_p, & \tau = p \end{cases} \tag{A.5}$$

$$\frac{d^2\Gamma^{-1}}{dR(\tau)^2} = \begin{cases} -\dfrac{d\mathbf{\Gamma}^{-1}}{dR(\tau)}\ \text{toeplitz}\,(e_{\tau+1})\mathbf{\Gamma}^{-1} & \\ -\mathbf{\Gamma}^{-1}\ \text{toeplitz}\,(e_{\tau+1})\dfrac{d\mathbf{\Gamma}^{-1}}{dR(\tau)}, & \\ \qquad 0 \le \tau \le p-1 \\ \mathbf{0}, \qquad \tau = p. \end{cases} \tag{A.6}$$

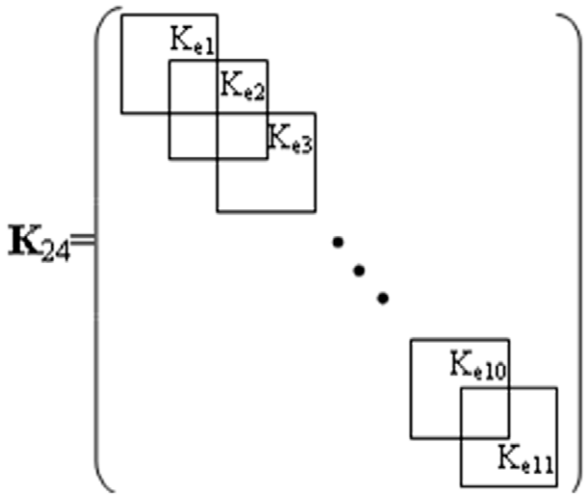

Figure B.1. The global stiffness matrix $\mathbf{K}_{24}$.

Appendix B. Sensitivity of the global stiffness matrix of the simply supported bridge system with respect to changes in the element sectional stiffness

To form the global stiffness matrix, the FEM nodes should be identified and the 11 element stiffness matrices be assembled by placing the terms associated with the same nodal DOF together and summing them. Here beam elements with no axial elongation are employed.

Thus for the 10-DOF case the global stiffness matrix is first formed as a 24 × 24 matrix (figure B.1), corresponding to the 12 nodes of the system (including the boundary nodes). Static condensation is performed on $\mathbf{K}_{24}$ to eliminate the massless rotational DOFs to get the final stiffness matrix $\mathbf{K}_{\mathrm{f}}$. Define $\boldsymbol{\xi}$ and $\boldsymbol{\eta}$ to be sets of certain indices of the rows and columns of the matrix $\mathbf{K}_{24}$ and the notation $\mathbf{K}_{24}(\boldsymbol{\xi}, \boldsymbol{\eta})$ stands for the submatrix that consists of the terms in rows $\boldsymbol{\xi}$ and columns $\boldsymbol{\eta}$. Since the translational displacements at beam ends are zero, the 1st and 23rd row and column of $\mathbf{K}_{24}$ will be left out of consideration:

$$\mathbf{K}_{\mathrm{f}} = \mathbf{K}_{mm} - \mathbf{K}_{m0}\mathbf{K}_{00}^{-1}\mathbf{K}_{0m}, \tag{B.1}$$

$$\mathbf{K}_{mm} = \mathbf{K}_{24}(\mathbf{i}, \mathbf{i}); \qquad \mathbf{K}_{m0} = \mathbf{K}_{24}(\mathbf{i}, \mathbf{j});$$
$$\mathbf{K}_{00} = \mathbf{K}_{24}(\mathbf{j}, \mathbf{j});$$
$$\mathbf{K}_{0m} = \mathbf{K}_{m0}^{\mathrm{T}} = \mathbf{K}_{24}(\mathbf{j}, \mathbf{i}).$$
$$\mathbf{i} = 3, 5, \ldots, 21 \text{ (odd number collection)},$$
$$\mathbf{j} = 2, 4, \ldots, 24 \text{ (even number collection)}. \tag{B.2}$$

To calculate the derivative of $\mathbf{K}_{24}$ with respect to element sectional stiffness $(EI)_i$ (i is the label of the element), take the derivative of the element stiffness matrix $(\mathbf{K}_{\mathrm{e}})_i$ over $(EI)_i$ and use a congruent transformation to map the local coordinates to the global coordinates:

$$\frac{\mathrm{d}\mathbf{K}_{24}}{\mathrm{d}(EI)_i} = \begin{bmatrix} \mathbf{0}_{(2i-2)\times 4} \\ \mathbf{I}_{4\times 4} \\ \mathbf{0}_{(22-2i)\times 4} \end{bmatrix}_{24\times 4} \frac{\mathrm{d}(\mathbf{K}_{\mathrm{e}})_i}{\mathrm{d}(EI)_i} \times [\mathbf{0}_{4\times(2i-2)}, \mathbf{I}_{4\times 4}, \mathbf{0}_{4\times(22-2i)}]_{4\times 24}, \quad i = 1{:}11. \tag{B.3}$$

The sensitivities of $\mathbf{K}_{mm}$, $\mathbf{K}_{m0}$, $\mathbf{K}_{0m}$ and $\mathbf{K}_{00}$ can be obtained by substituting equation (B.3) into (B.2):

$$\therefore \frac{\mathrm{d}\mathbf{K}_{mm}}{\mathrm{d}(EI)_i} = \begin{cases} \begin{bmatrix} [0010] \\ \mathbf{0}_{9\times 4} \end{bmatrix}_{10\times 4} \frac{\mathrm{d}(\mathbf{K}_{\mathrm{e}})_1}{\mathrm{d}(EI)_1} \begin{bmatrix} [0010] \\ \mathbf{0}_{9\times 4} \end{bmatrix}_{10\times 4}^{\mathrm{T}}, & i = 1 \\ \begin{bmatrix} \mathbf{0}_{(i-2)\times 4} \\ [1000] \\ [0010] \\ \mathbf{0}_{(10-i)\times 4} \end{bmatrix}_{10\times 4} \frac{\mathrm{d}(\mathbf{K}_{\mathrm{e}})_i}{\mathrm{d}(EI)_i} \begin{bmatrix} \mathbf{0}_{(i-2)\times 4} \\ [1000] \\ [0010] \\ \mathbf{0}_{(10-i)\times 4} \end{bmatrix}_{10\times 4}^{\mathrm{T}}, & i = 2{:}10 \\ \begin{bmatrix} \mathbf{0}_{9\times 4} \\ [1000] \end{bmatrix}_{10\times 4} \frac{\mathrm{d}(\mathbf{K}_{\mathrm{e}})_{11}}{\mathrm{d}(EI)_{11}} \begin{bmatrix} \mathbf{0}_{9\times 4} \\ [1000] \end{bmatrix}_{10\times 4}^{\mathrm{T}}, & i = 11, \end{cases} \tag{B.4}$$

$$\frac{\mathrm{d}\mathbf{K}_{m0}}{\mathrm{d}(EI)_i} = \left(\frac{\mathrm{d}\mathbf{K}_{0m}}{\mathrm{d}(EI)_i}\right)^{\mathrm{T}} = \begin{cases} \begin{bmatrix} [0010] \\ \mathbf{0}_{9\times 4} \end{bmatrix}_{10\times 4} \frac{\mathrm{d}(\mathbf{K}_{\mathrm{e}})_1}{\mathrm{d}(EI)_1} \begin{bmatrix} [0100] \\ [0001] \\ \mathbf{0}_{10\times 4} \end{bmatrix}_{12\times 4}^{\mathrm{T}}, & i = 1 \\ \begin{bmatrix} \mathbf{0}_{(i-2)\times 4} \\ [1000] \\ [0010] \\ \mathbf{0}_{(10-i)\times 4} \end{bmatrix}_{10\times 4} \frac{\mathrm{d}(\mathbf{K}_{\mathrm{e}})_i}{\mathrm{d}(EI)_i} \begin{bmatrix} \mathbf{0}_{(i-1)\times 4} \\ [0100] \\ [0001] \\ \mathbf{0}_{(11-i)\times 4} \end{bmatrix}_{12\times 4}^{\mathrm{T}}, & i = 2{:}10 \\ \begin{bmatrix} \mathbf{0}_{9\times 4} \\ [1000] \end{bmatrix}_{10\times 4} \frac{\mathrm{d}(\mathbf{K}_{\mathrm{e}})_{11}}{\mathrm{d}(EI)_{11}} \begin{bmatrix} \mathbf{0}_{10\times 4} \\ [0100] \\ [0001] \end{bmatrix}_{12\times 4}^{\mathrm{T}}, & i = 11 \end{cases} \tag{B.5}$$

$$\frac{\mathrm{d}\mathbf{K}_{00}}{\mathrm{d}(EI)_i} = \begin{bmatrix} \mathbf{0}_{(i-1)\times 4} \\ [0100] \\ [0001] \\ \mathbf{0}_{(11-i)\times 4} \end{bmatrix}_{12\times 4} \frac{\mathrm{d}(\mathbf{K}_{\mathrm{e}})_i}{\mathrm{d}(EI)_i} \begin{bmatrix} \mathbf{0}_{(i-1)\times 4} \\ [0100] \\ [0001] \\ \mathbf{0}_{(11-i)\times 4} \end{bmatrix}_{12\times 4}^{\mathrm{T}}, \quad i = 1{:}11. \tag{B.6}$$

Finally, the sensitivity of the condensed global stiffness matrix $\mathbf{K}_{\mathrm{f}}$ to stiffness reduction for element i is computed by differentiating both sides of equation (B.1) with respect to $(EI)_i$ and substituting equations (B.4)–(B.6) into that expression:

$$\frac{\mathrm{d}\mathbf{K}_{\mathrm{f}}}{\mathrm{d}(EI)_i} = \frac{\mathrm{d}\mathbf{K}_{mm}}{\mathrm{d}(EI)_i} - \mathbf{K}_{m0}K_{00}^{-1}\frac{\mathrm{d}\mathbf{K}_{0m}}{\mathrm{d}(EI)_i} - \frac{\mathrm{d}\mathbf{K}_{m0}}{\mathrm{d}(EI)_i}\mathbf{K}_{00}^{-1}\mathbf{K}_{0m} + \mathbf{K}_{m0}\mathbf{K}_{00}^{-1}\frac{\mathrm{d}\mathbf{K}_{00}}{\mathrm{d}(EI)_i}\mathbf{K}_{00}^{-1}\mathbf{K}_{0m}. \tag{B.7}$$

References

[1] Doebling S W, Farrar C R and Prime M B 1998 A summary review of vibration-based damage identification methods *Shock Vib. Dig.* **30** 91–105

[2] Ciang C C, Lee J R and Bang H J 2008 Structural health monitoring for a wind turbine system: a review of damage detection methods *Meas. Sci. Technol.* **19** 122001

[3] Peeters B, Maeck J and De Roeck G 2001 Vibration-based damage detection in civil engineering: excitation sources and temperature effects *Smart Mater. Struct.* **10** 518

[4] Lynch J P, Sundararajan A, Law K H, Kiremidjian A S and Carryer E 2004 Embedding damage detection algorithms in a wireless sensing unit for operational power efficiency *Smart Mater. Struct.* **13** 800

[5] Maia N M M, Silva J M M, Almas E A M and Sampaio R P C 2003 Damage detection in structures: from mode shape to frequency response function methods *Mech. Syst. Signal Process.* **17** 489–98

[6] Hearn G and Testa R B 1991 Modal analysis for damage detection in structures *J. Struct. Eng.* **117** 3042–63

[7] Salawu O S 1997 Detection of structural damage through changes in frequency: a review *Eng. Struct.* **19** 718–23

[8] Worden K, Manson G and Fieller N R J 2000 Damage detection using outlier analysis *J. Sound Vib.* **229** 647–67

[9] Okafor A C and Dutta A 2000 Structural damage detection in beams by wavelet transforms *Smart Mater. Struct.* **9** 906

[10] Fang X, Luo H and Tang J 2005 Structural damage detection using neural network with learning rate improvement *Comput. Struct.* **83** 2150–61

[11] Brockwell P J and Davis R A 2009 *Time Series: Theory and Methods* (Berlin: Springer)

[12] Sohn H and Farrar C R 2001 Damage diagnosis using time series analysis of vibration signals *Smart Mater. Struct.* **10** 446

[13] Zhang Q W 2007 Statistical damage identification for bridges using ambient vibration data *Comput. Struct.* **85** 476–85

[14] Yao R and Pakzad S N 2012 Autoregressive statistical pattern recognition algorithms for damage detection in civil structures *Mech. Syst. Signal Process.* **31** 355–68

[15] Nair K K, Kiremidjian A S and Law K H 2006 Time series-based damage detection and localization algorithm with application to the ASCE benchmark structure *J. Sound Vib.* **291** 349–68

[16] Atamturktur S, Bornn L and Hemez F 2011 Vibration characteristics of vaulted masonry monuments undergoing differential support settlement *Eng. Struct.* **33** 2472–84

[17] Gul M and Necati Catbas F 2009 Statistical pattern recognition for structural health monitoring using time series modeling: theory and experimental verifications *Mech. Syst. Signal Process.* **23** 2192–204

[18] Dorvash S and Pakzad S N 2012 Effects of measurement noise on modal parameter identification *Smart Mater. Struct.* **21** 065008

[19] Mahalanobis P C 1936 On the generalized distance in statistics *Proc. Natl Acad. Inst. Sci. India* **2** 49–55

[20] Gray A Jr and Markel J 1976 Distance measures for speech processing *IEEE Trans. Acoust. Speech Signal Process.* **24** 380–91

[21] Brockwell P J and Richard A D 2002 *Introduction to Time Series and Forecasting* (London: Taylor & Francis)

[22] Chopra A K 2006 *Dynamics of Structures: Theory & Applications to Earthquake Engineering* (Upper Saddle River, NJ: Prentice-Hall)

[23] Teräsvirta T 1977 The invertibility of sums of discrete MA and ARMA processes *Scand. J. Stat.* **4** 165–70

[24] Porat B 1994 *Digital Processing of Random Signals: Theory and Methods* (Englewood Cliffs, NJ: Prentice-Hall)

[25] Oppenheim A V, Schafer R W and Buck J R 2009 *Discrete-Time Signal Processing* 3rd edn (Upper Saddle River: Prentice-Hall)

[26] James G H III, Carne T G and Lauffer J P 1993 *The Natural Excitation Technique (NExT) for Modal Parameter Extraction from Operating Wind Turbines* No. SAND-92-1666 (Albuquerque, NM: Sandia National Labs)

[27] Berk K N 1974 Consistent autoregressive spectral estimates *Ann. Statist.* **2** 489–502

[28] Pakzad S N, Kim S, Fenves G L, Glaser S D, Culler D E and Demmel J W 2005 Multi-purpose wireless accelerometers for civil infrastructure monitoring *IWSHM 2005: 5th Int. Workshop on Structural Health Monitoring (Stanford, CA)*

[29] Wang Y, Lynch J P and Law K H 2007 A wireless structural health monitoring system with multithreaded sensing devices: design and validation *Struct. Infrastruct. Eng.* **3** 103–20